La mer 35: 85-93, 1997
Société franco-japonaise d'océanographie, Tokyo

Co-tidal and co-range charts in the South China Sea derived from satellite altimetry data

Tetsuo YANAGI*, Toshiyuki TAKAO* and Akihiko MORIMOTO*

Abstract: Co-tidal and co-range charts of major six tidal constituents, M_2, S_2, K_1, O_1, P_1 and S_a in the South China Sea are drawn from the results of the harmonic analysis of TOPEX/POSEIDON altimetric data and tide gauge data along the coast. Those of M_2 and K_1 constitutents agree well with the existing ones estimated from only tide guage data at coastal stations. Those of S_2 are similar to those of M_2 and those of O_1 and P_1 are similar to those of K_1. The amplitude of S_a constitutent is large at the northeastern and southwestern parts of the South China Sea and its phase differs 180° on both sides. There are two amphidromic points of S_a constitutent off the Vietnam Coast.

1. Introduction

The South China Sea is a marginal sea with the shallow parts less than 200 m in the Gulfs of Thailand and Tongking and the deep part of about 4000 m at the central region (Fig. 1a). The characteristics of tidal wave in the South China Sea have been investigated by FANG (1986) and HUANG *et al.* (1994) and the numerical experiment on tidal wave propagation there was carried out by YE and ROBINSON (1983). In recent years, MAZZEGA and BERGE (1994) drew the co-tiral and co-range charts of eight leading tidal constituents (M_2, S_2, N_2, K_2, K_1, O_1, P_1 and Q_1) in the South China Sea by inverting combined sets of tide gauge harmonic constants and a reduced sets of TOPEX /POSEIDON satellite alitimetric data. On the other hand, YANAGI *et al.* (1997) succeeded to clarify the characteristics of tidal phenomena in the East China Sea and the Yellow Sea by the harmonic analysis of the altimetric data from TOPEX/POSEIDON.

In this paper, we try to reveal the characteristics of major six tidal constituents (M_2, S_2, K_1, O_1, P_1 and S_a)in the South China Sea with use of the altimetric data from TOPEX/POSEIDON on the basis of the method developed by YANAGI *et al.* (1997) and compare our results with the existing tidal charts by FANG (1986) and MAZZEGA and BERGE (1994).

*Department of Civil and Ocean Engineering, Ehime University, Matsuyama 790, Japan

2. Altimetric data

The satellite TOPEX/POSEIDON was launched in August 1992 and has continued to obtain the altimetric data every about 10 days along 17 observation lines in the South Chaina Sea as shown in Fig. 1 (b). The data are provided as Merged Geophysical Data Record (MGDR) by the Physical Oceanogrphy Distributed Active Archive Center at Jet Propulsion Laboratory, U.S.A. We use the data by only TOPEX alimeter from Cycle 1 (September 1992) until Cycle 101 (June 1994) in this analysis. Since POSEIDON altimeter had unkown bias of the order of 20 cm to TOPEX one, we did not use the data by PSEIDON altimeter in this study (This problem was solved by NASA in July 1996 and we can use also PSEIDON data now).

Standard data correction including electromagnetic bias correction, ionospheric correction, dry and wet trospheric correction and solid earth tide correction were made using the values provided in the MGDR. However we do not carry out any procedure to remove the radial orbit error because the tidal component may be missing by this correction. The radial orbit error has a wave length of circumference of the earth and has the value of about 3 cm (FU *et al.*, 1994). This is very small compared to the tidal signal in the South Chinal Sea and

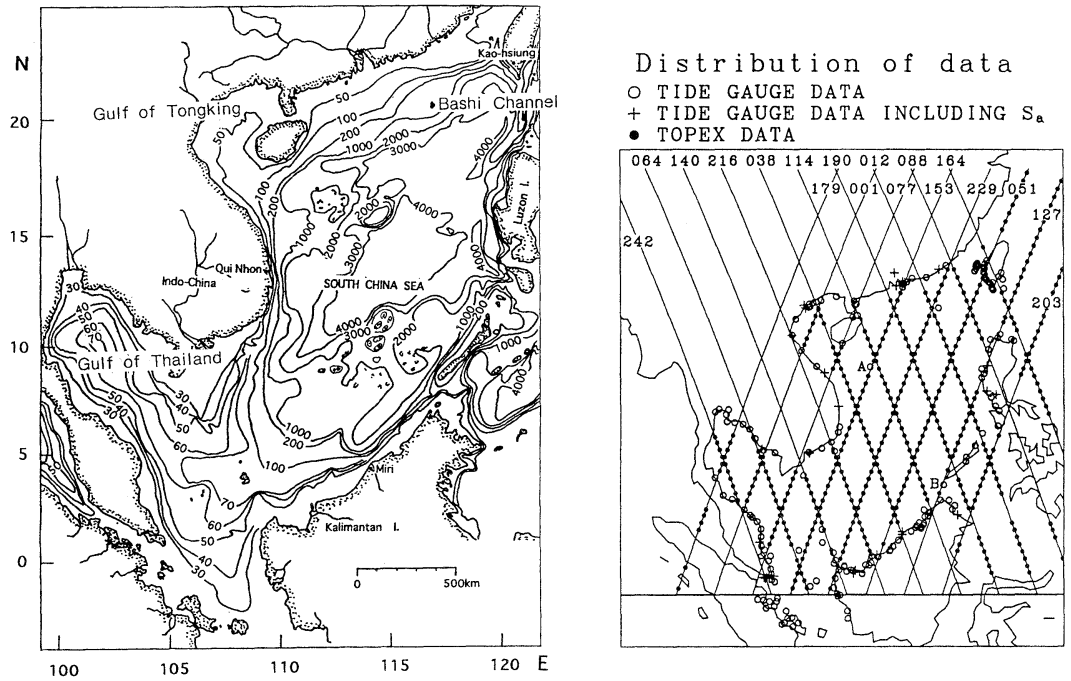

Fig. 1. The South China Sea (a) and the observation lines of TOPEX/POSEIDON and tide guage stations (b). A and B denote the points where the results by TOPEX altimetric data are compared with the tide guage data.

other improtant signal related to the sea surface dynamic topography may be missed by this correction.

The data of both ascending and descending tracks are used after editing the data to remove the abnormal values by the malfunction of instrument. Next we remove the extreme altimetric values larger than ± 3 m from the temporal mean of all data because the maximum spring tidal amplitude becomes about 2 m in the South Chaina Sea (HUANG *et al.*, 1994). Data are originally obtained every about 1 second; every about 6.2 km along the satellite tracks but the data points differ every mission. Hence we linearly interpolated every data at the fixed points with 6.2 km interval along the subsatellite track which is the projection of satellite track on the sea surface as shown in Fig. 1 (b).

The altimetry data after the initial correction $S(r, t)$ is expressed by the followings,

$$S(r, t) = \eta(r) + \eta^*(r, t) \quad (1)$$

Here $\eta(r)$ denotes the temporal mean of all data at station r, $\eta^*(r, t)$ the temporal deviation which includes the temporal variation of sea surface dynamic topography, tide, temporal variation of radial orbit error and measurement error. We use $\eta^*(r, t)$ for the harmonic analysis.

3. Harmonic analysis

Tidal amplitudes at three representative stations along the coast in the South China Sea: Kao-Hsing, Qui-Nhon and Miri (see Fig. 1), are shown in Fig. 2 (Tidal harmonic constants are kindly provided by the Japan Oceanographic Data Center). The K_1 constituent is the most dominant one and it is 36.0 cm at Miri, 32.9 cm at Qui-Nhon and 15.6 cm at Kao-Hsiung. We consider the tidal constituents whose amplitude are larger than 7 cm in this analysis, i.e. S_a, K_1, O_1, P_1, M_2 and S_2, because the accuracy of TOPEX/POSEIDON altimeter is about 5 cm (FU *et al.*, 1994).

At first we did not include S_a constituent in this analysis but we could not obtain accurate harmonic constants because it has large

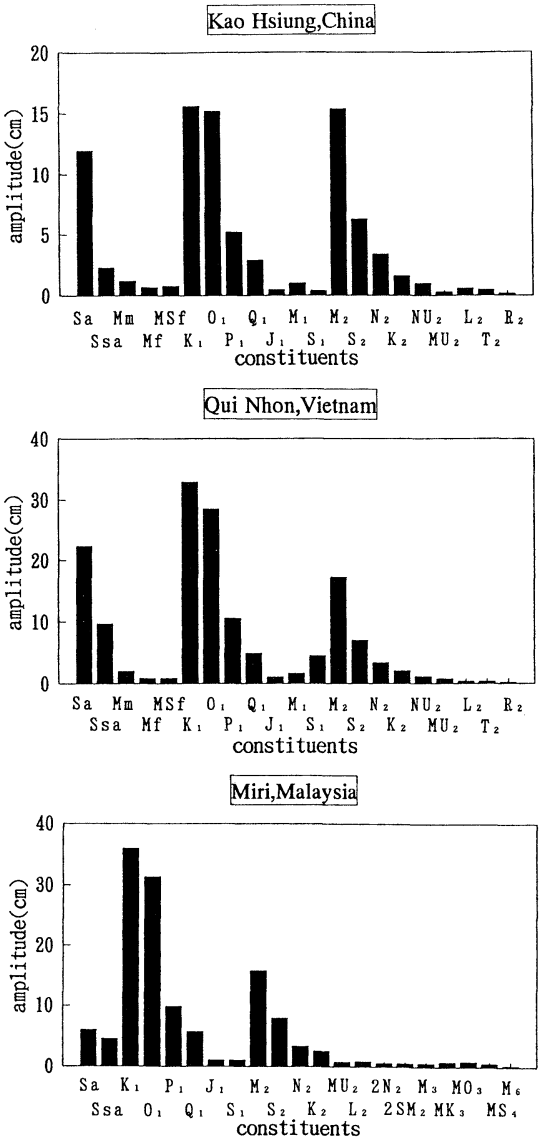

Fig. 2 Tidal amplitudes at three representative tide gauge stations along the coast of the South China Sea.

amplitude in this area as shown in Fig. 2. Then we include S_a constituent in this harmonic analysis though it is not an astronomical tidal constituent but a meteorological one.

The tidal harmonic analysis in this study is carried out with use of the aliasing period from each tidal constituent except S_a because the sampling time of about 10 days by TOPEX is much longer than tidal period of each constituent, that is, semi-diurnal or diurnal periods.

Tabel 1. Tidal periods and aliasing periods of major tidal consituents.

Tides	Period(hours)	Aliasing Period(days)
M_2	12.420601	62.10
S_2	12.	58.74
K_1	23.93447	173.22
O_1	25.819342	45.71
P_1	24.06589	88.89
S_a	8765.821 (365.245 days)	

The aliasing period T_a from each tidal frequency f is calculated by the follwing formula,

$$T_a = 1/(2nf_c \pm f) \qquad (2)$$
$$f_c = 1/2\Delta t$$

where n denotes a integer part of $t \times f$($n=19$ for M_2 tidal constituent), f_c the Nyquist frequency and Δt the sampling interval 9.9156 days. The shortest aliasing period from each semi-diurnal and diurnal constituent is shown in Table 1. We have to pay an attention to the fact that the accuracy of the period is critical for this harmonic analysis because T_a largely changes according to the small change of Δt. This means that we have to use the double precision scheme in the computation (10^{-6} in this case). The necessary sampling time T_d for separating two tidal constituents, whose aliasing periods T_1 and T_2 are close, is calculated by the following fromula

$$T_d = T_1 \times T_2/(T_1 - T_2)/4 \qquad (3)$$

where T_1 is longer than T_2 and the number of 4 means that the 1/4 wave length is necessary at least for the separation of two constituents. From this formula we understand that 0.7 year (277.1 days) is necessary for separating M_2 and S_2 constituents and 51.5 days for separating S_2 and O_1 constituents in the altimetric data. The observation period of about 1000 days in this study is sufficient for the separation of six major tidal constituents.

The tidal harmonic analysis by the least square method is directly carried out with use of unknown amplitudes and phases of 6 constituents. We compare our results at A and B (see Fig. 1 b) with those obtained by the tide gauge observations at islands. The results are

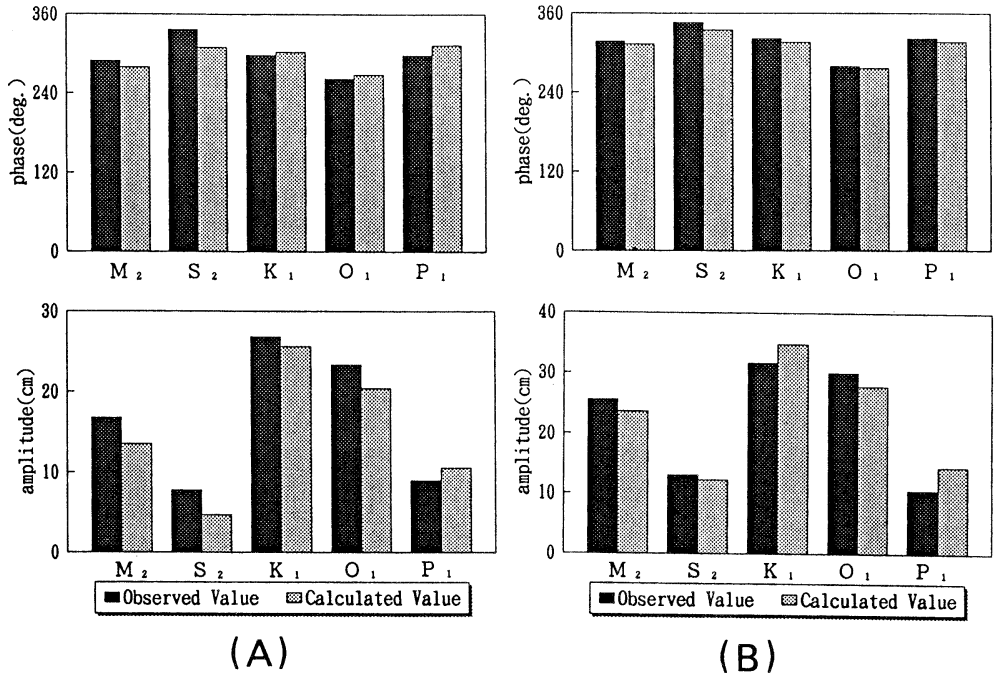

Fig. 3 Comparison of obtained tidal harmonics by TOPEX and tide gauge at A and B. Phase refers to the longitude of observation station.

shown in Fig. 3 except for S_a because there are not observed S_a tidal harmonics at A and B. The agreement between our results and observed ones by tide gauge stations is encouragingly close both for amplitude and phase, i.e. the difference of amplitudes is smaller than 5 cm which is the accuracy of TOPEX alitimeter.

4. Results

We draw the co-tidal and co-range charts of six tidal constituents in the South China Sea. At first tidal variation of the sea surface in the whole area by each tidal constituent is reconstructed with use of estimated tidal harmonics along the coast and those along the subsatellite tracks shown in Fig. 1 (b). The tidal variation of the sea surface except the subsatellite track are interpolated with use of the exponential function as follows,

$$\xi(x) = \frac{\sum_i W(x, r_i)\tau(r_i)}{\sum_i W(x, r_i)} \qquad (4)$$

$$W(x, r_i) = \exp\left\{\frac{(r_i - x)^2}{L^2}\right\}$$

where $\xi(x)$ denotes the interpolated sea surface height, x the position of interpolation, r_i the position where tidal harmonics are already obtained, $\tau(r_i)$ the sea surface height at r_i and L (=185km) the decorrelation radius, which is decided by the distance of neighboring subsatellite tracks. The interpolation is carried out at every $0.5° \times 0.5°$ mesh point. If there are not two observation stations within the circle of $1.5 \times L$, the interpolation is not carried out at that point. After the estimation of temporal variation of sea surface height in one tidal cycle, we carry out the tidal harmonic analysis at every $0.5° \times 0.5°$ mesh point in the whole area and obtained tidal harmonics there.

The obtained co-range and co-tidal charts of M_2 constituent are shown in Fig. 4 (a) and (b) with those estimated by FANG (1986) and MAZZEGA and BERGE (1994). The agreement of three figures are good with small discrepancies. The positions of amphidromic point at the central part of the Gulf of Thailand by ours and by FANG (1986) are nearly the same but that by MAZZEGA and BERGE (1994) is a little different. There is no amphidromic point between

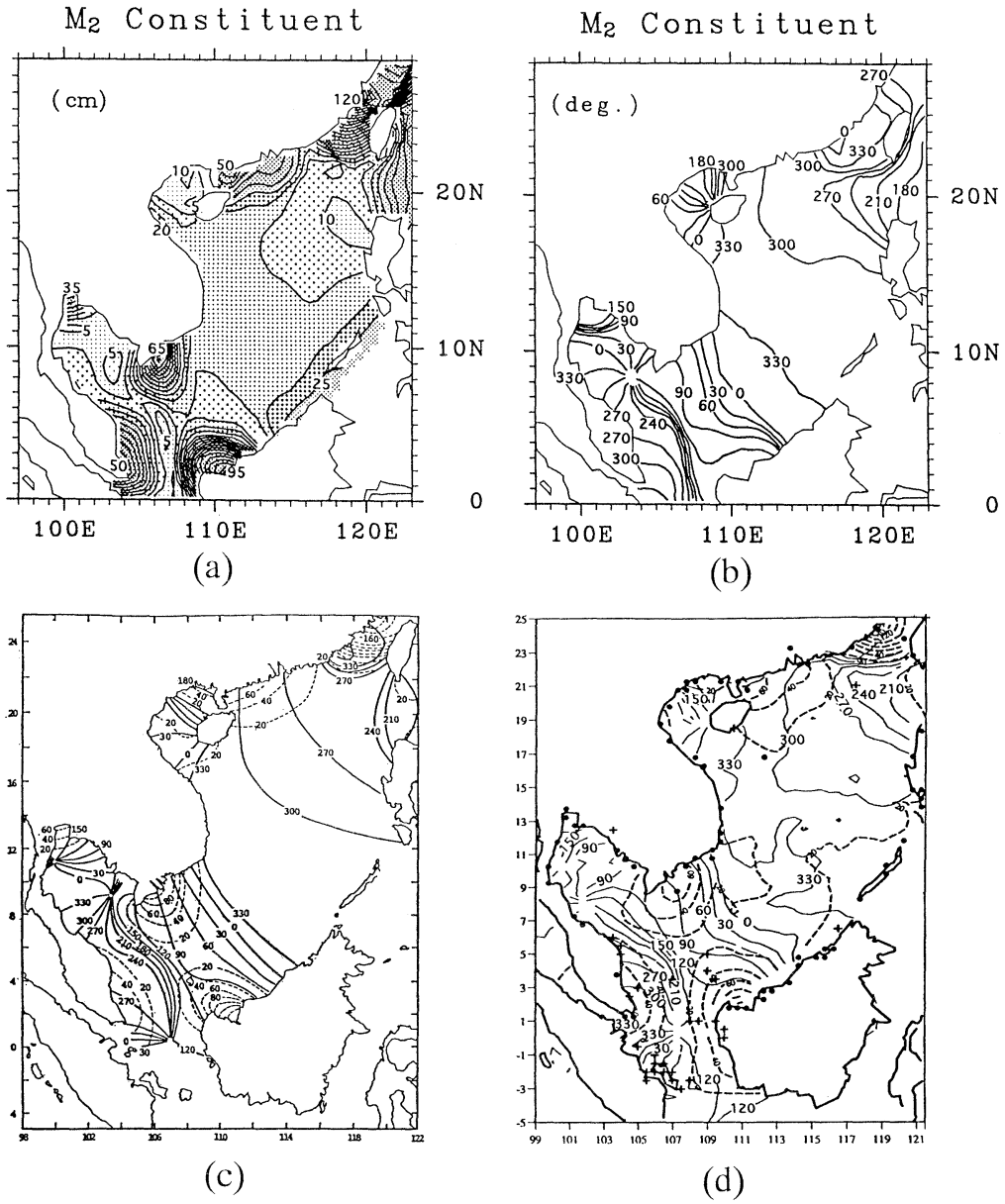

Fig. 4 Co-range (a) and co-tidal (b) charts of M_2 constituent by TOPEX and those by Fang (1986) (c) and those by Mezzega and Berge (1994) (b). Phase refers to 135° E.

the Malay peninsula and Borneo island only by our result and this is due to that it is located near the boundary of our analysis area. Another amphidromic point exists at the head of Gulf of Thailand by FANG (1986) but there is no amphidromic point by ours and MAZZEGA and BERGE (1994). Those of K_1 constituent are shown in Fig. 5 (a) and (b) with those estimated by FANG (1986) and MAZZEGA and BERGE (1994). The agreement of three figures are good except that the co-range charts at the central part of the South China Sea are different. The 30 cm amplitude line runs from west to east by FANG (1986) and MAZZEGA and BERGE (1994) but it runs from north to south by ours.

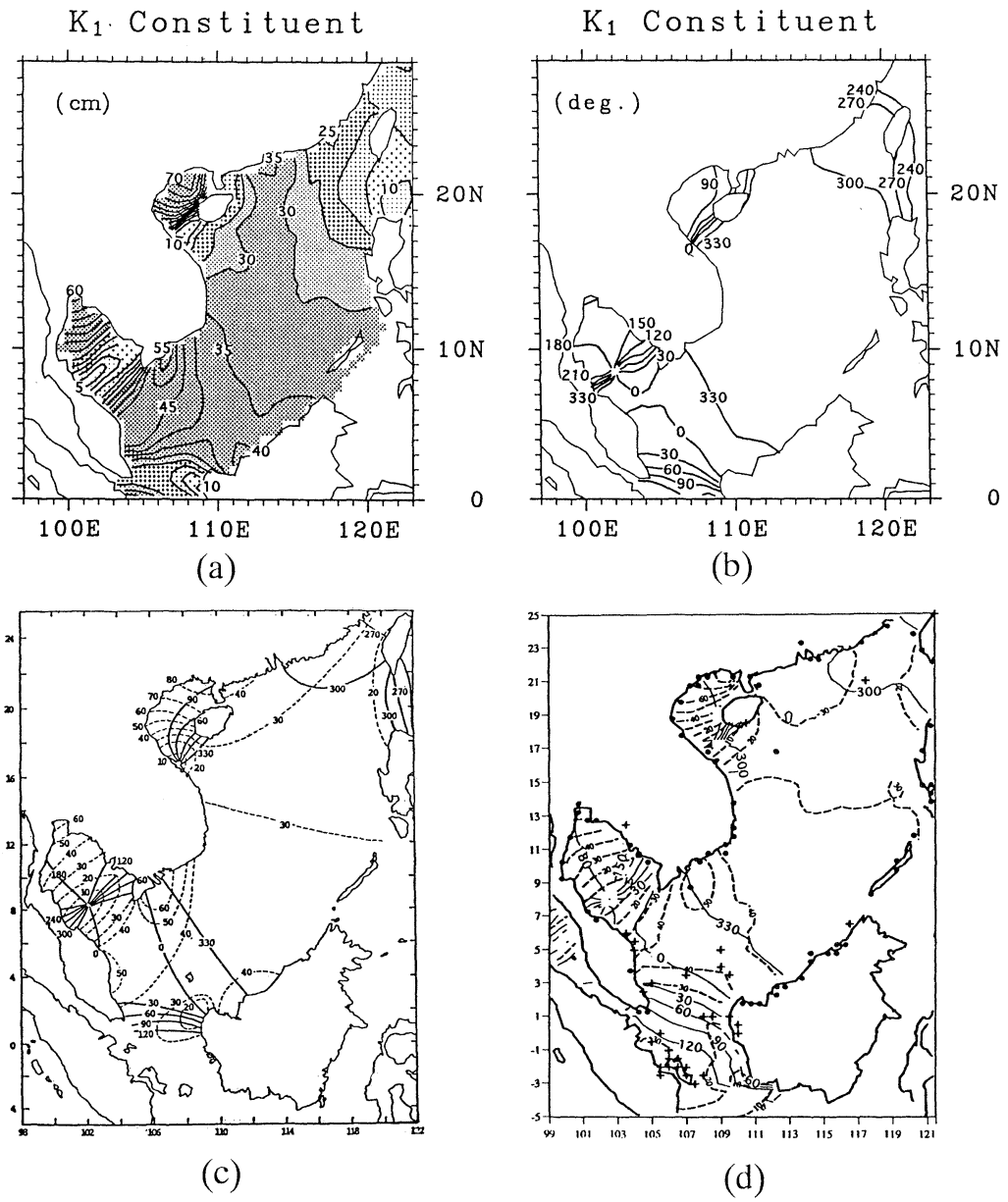

Fig. 5 Same as Fig. 4 except K_1 constituent.

The co-tidal and co-range charts of other three constituents, S_2, O_1 and P_1 are shown in Fig. 6 without those by existing charts because there are no published charts for these three constituents. Those of S_2 constituent are similar to those of M_2 and those of O_1 and P_1 to K_1, respectively.

The co-range and co-tidal charts of S_a constituent are shown in Fig. 7 and its amplitude is large in the northeastern and southwestern parts of the South China Sea. The phase in both sides differ by about 180°. There are two amphidromic points off southeastern Vietnam coast.

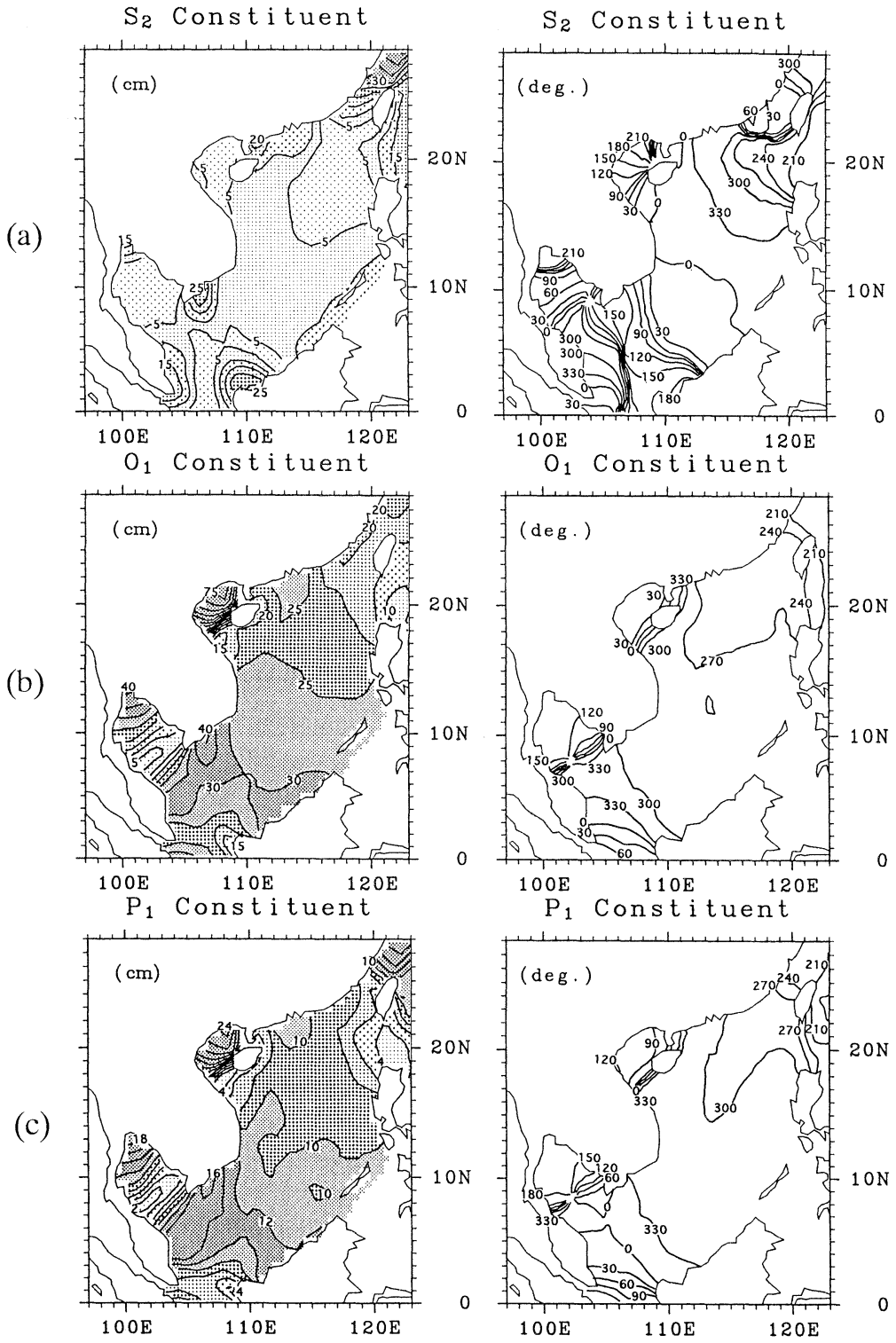

Fig. 6 Co-range and co-tidal charts of S_2 (a), O_1(b) and P_1 (c) constituents. Phase refers to 135° E.

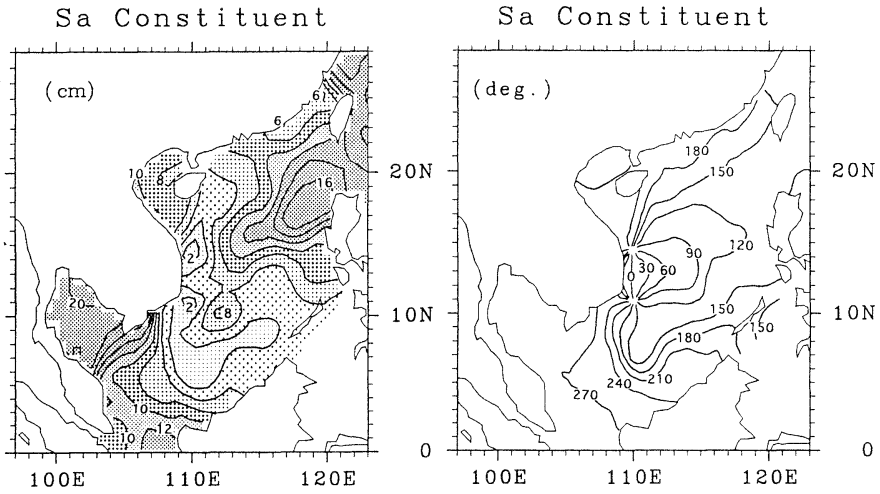

Fig. 7 Co-range and co-tidal charts of S_a constituent.

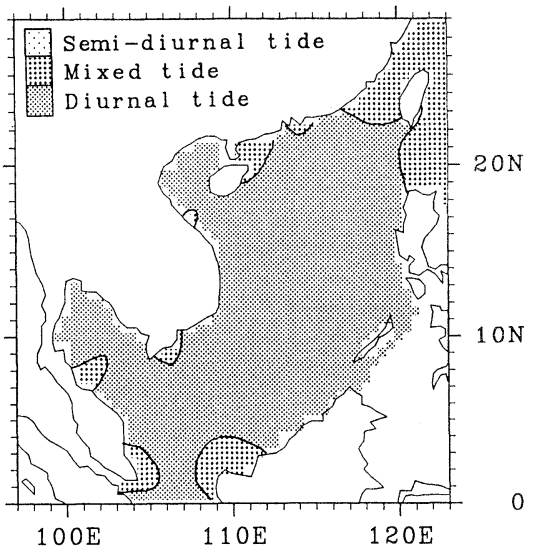

Fig. 8 Horizontal distribution of tidal type in the South China Sea.

5. Discussions

The horizontal distribution of tidal type $F\{=(H_{K1}+H_{O1})/(H_{M2}+H_{S2})$ in which H means the amplitude} in the South China Sea obtained by the present study on the basis of altimetric data and tide gauge data is shown in Fig. 8. The diurnal type is defined as F>1.25, the semidiuranal type as F<0.25 and the mixed type as 1.25>F>0.25. There is no region where the semidiurnal tide dominates and the diurnal tide dominates nearly in the whole region of the South China Sea. The M_2 and K_1 tidal waves mainly intrude from the Pacific Ocean through Bashi Channel with nearly the same amplitude of about 10 cm and propagate southwestward but the amplitude of K_1 tide is larger (about 30 cm) than that of M_2 tide (about 15 cm) at the central part in the South China Sea as shown in Fig (4) and (5). This may be accounted for the resonance, that is, the natural oscillating period (T_n) of the South China Sea is near the diurnal period. The first mode of T_n of the South China Sea (T_{n1}) is calculated by

$$T_{n1} = 4L/\sqrt{(gh)} \qquad (5)$$

where L(=2500 km) denotes the length from Bashi Channel to the east coast of Malay Peninsula, g (=9.8 ms^{-2}) the gravitaional acceralation and h (=1500 m) the mean depth of the South China Sea. Estimated T_{n1} from Eq (5) is 22.9 hours and near to the diurnal period. The co-phase lines of K_1 constituent are crowded at Bashi Channel and the node of standing wave is situated here. The phase difference of K_1 constituent between the Bashi Channel and the eart coast of Malay Peninsula is near 90° as shown in Fig 5 (b). The characteristics of O_1 and P_1 constituents are nearly the same as K_1 as shown in Fig. 6.

The phase of 140° of S_a constituent means mid August because it refers to Vernal Equinox Day (around 21 March) and S_a constituent takes its maximum in August at the northeastern part and in December at the southwestern part. These facts suggest that the main cause of S_a constituent in the South China Sea is the monsoon wind blowing, that is, the southwest monsoon wind in boreal summer piles up the water at the northeastern part and the northeast monsoon wind in boreal winter piles up the water at the southwestern part of the South China Sea. The maximum amplitude of S_a constituent is appeared off Luson Island and the head of Gulf of Thailand and these areas are situated at the right hand side to the downwind direction. This may be due to the surface Ekman transport.

The local amplification mechanisms of diurnal of semi-diurnal constituents, the generation mechanism of amphidromic points in the Gulfs of Thailand and Tongking and the reason of a small difference between our charts and those by FANG (1986) and MAZZEGA and BERGE (1994) will be discussed in the succeeding paper with use of numerical experiments.

Acknowledgement

The authors express their sincere thanks to Drs. H. TAKEOKA and K. ICHIKAWA of Ehime University for their frutiful discussion.

References

FANG, G. (1986): Tide and tidal current charts for the marginal seas adjacent China. Chin. J. of Oceanology and Limnology, **4**, 1–16.

FU, L., E. J. CHRISTENSEN, C. A. YAMARONE Jr., M. LEFEBRE, Y. MENARD, M. DORRER and P. E SCUDIER (1994): TOPEX/POSEIDON mission overview. J. Geophys. Res., **99**, C12, 24, 369–24, 381.

HUANG, Q., W. WANG and J. CHEN (1994): Tides, tidal currents and storm surge set-up of South China Sea. *In* Oceanlogy of China Sea, Vol. 1, ZHOU, D. *et al.*, (ed), Kluwer Academic Publisher, 113–122.

MAZZEGA, P. and M. BERGE (1994): Ocean tides in the Asian semienclosed sea from TOPEX/POSEIDON. J. Geophy. Res., **99**, C12, 24, 867–24, 881.

YANAGI, T., A. MORIMOTO and K. ICHIKAWA(1997): Co-tidal and co-range charts for the East China Sea and the Yellow Sea derived from satellite altimetry data. J. Oceanogr., **53**, 303–309.

YE, A. L. and I. S. ROBINSON (1983): Tidal dynamics in the South China Sea. Geophys. J.R. astr. Soc., **72**, 691–707.

Received August 20, 1996
Accepted May 8, 1997